Supplement of Earth Syst. Sci. Data, 16, 277–293, 2024
https://doi.org/10.5194/essd-16-277-2024-supplement

Open Access Earth System Science Data

Supplement of

Mapping 24 woody plant species phenology and ground forest phenology over China from 1951 to 2020

Mengyao Zhu et al.

Correspondence to: Junhu Dai (daijh@igsnrr.ac.cn) and Quansheng Ge (geqs@igsnrr.ac.cn)

Table S1: List of 12 bioclimatic layers selected as environmental data inputs for the species distribution model.

No.	Short name	Long name	Unit	Explanation
1	bio1	mean annual air temperature	°C	mean annual daily mean air temperatures averaged over 1 year
2	bio2	mean diurnal air temperature range	°C	mean diurnal range of temperatures averaged over 1 year
3	bio3	isothermality	°C	ratio of diurnal variation to annual variation in temperatures
4	bio5	mean daily maximum air temperature of the warmest month	°C	the highest temperature of any monthly daily mean maximum temperature
5	bio6	mean daily minimum air temperature of the coldest month	°C	the lowest temperature of any monthly daily mean maximum temperature
6	bio12	annual precipitation amount	kg m^{-2}	accumulated precipitation amount over 1 year
7	gdd5	growing degree days heat sum above 5°C	°C	heat sum of all days above the 5°C temperature accumulated over 1 year
8	gdd10	growing degree days heat sum above 10°C	°C	heat sum of all days above the 10°C temperature accumulated over 1 year
9	gsp	accumulated precipiation amount on growing season days TREELIM	kg m^{-2}	precipitation sum accumulated on all days during the growing season based on TREELIM (https://doi.org/10.1007/s00035-014-0124-0)
10	hurs_mean	mean monthly near-surface relative humidity	%	average monthly near-surface relative humidity over 1 year
11	rsds_mean	mean monthly surface downwelling shortwave flux in air	MJ m^{-2} d^{-1}	average monthly surface downwelling shortwave flux in air over 1 year
12	rsds_range	annual range of monthly surface Downwelling shortwave flux in air	MJ m^{-2} d^{-1}	difference between maximum and minimum monthly surface downwelling shortwave flux in air

Table S2: List of simulated data and results of species distribution for 24 species. Number of records represents the total number of occurrence records used when simulating the distribution of each species. AUC represents the area under the ROC curve, which indicates the accuracy of the simulation results of species distribution.

No.	Species	Family	Life form	Number of records	AUC
1	*Ginkgo biloba*	Ginkgoaceae	Tree	235	0.879
2	*Metasequoia glyptostroboides*	Cupressaceae	Tree	28	0.860
3	*Magnolia denudata*	Magnoliaceae	Tree	93	0.898
4	*Salix babylonica*	Salicaceae	Tree	240	0.773
5	*Populus* × *canadensis*	Salicaceae	Tree	17	0.747
6	*Robinia pseudoacacia*	Fabaceae	Tree	100	0.829
7	*Albizia julibrissin*	Fabaceae	Tree	124	0.890
8	*Cercis chinensis*	Fabaceae	Shrub	103	0.864
9	*Prunus armeniaca*	Rosaceae	Tree	165	0.822
10	*Ulmus pumila*	Ulmaceae	Tree	108	0.796
11	*Morus alba*	Moraceae	Tree	232	0.769
12	*Broussonetia papyrifera*	Moraceae	Tree	607	0.835
13	*Quercus acutissima*	Fagaceae	Tree	102	0.850
14	*Pterocarya stenoptera*	Juglandaceae	Tree	242	0.870
15	*Juglans regia*	Juglandaceae	Tree	195	0.826
16	*Betula platyphylla*	Betulaceae	Tree	229	0.886
17	*Acer pictum* subsp. *mono*	Sapindaceae	Tree	171	0.818
18	*Ailanthus altissima*	Simaroubaceae	Tree	241	0.837
19	*Melia azedarach*	Meliaceae	Tree	292	0.871
20	*Firmiana simplex*	Malvaceae	Tree	124	0.861
21	*Hibiscus syriacus*	Malvaceae	Shrub	268	0.868
22	*Fraxinus chinensis*	Oleaceae	Tree	253	0.825
23	*Syringa oblata*	Oleaceae	Shrub	76	0.902
24	*Paulownia fortunei*	Paulowniaceae	Tree	126	0.912
Total		-	-	4371	0.845

Table S3: Comparison results of GP maps and two LSP products in different forest type areas, which was made between FLD and SOS in spring and LCD and EOS in autumn within the time range 1981-2014 and 2013-2020. Forest type includes deciduous forest (DF), mix forest (MF), and evergreen forest (EF). LSP product includes VIPPHEN product (P1) and VNP22C2 product (P2). Method represents the aggregation method of GP maps, including mean, pct50, pct20\80 and pct10\90. *r*, RMSE, MAE, b_0, and n represents Pearson correlation coefficient, root mean square error, mean absolute error, linear regression slope, and number of comparing pixels, respectively.

Forest type	LSP product	GP vs. LSP	Method	*r*	RMSE	MAE	b_0	n
DF	P1	FLD-SOS	mean	0.830	25.3	23.5	0.452	3810
DF	P1	FLD-SOS	pct50	0.811	25.0	23.2	0.462	3809
DF	P1	FLD-SOS	pct20	0.809	21.1	18.0	0.375	3810
DF	P1	FLD-SOS	pct10	0.819	20.8	17.7	0.337	3810
DF	P2	FLD-SOS	mean	0.947	12.1	10.8	0.772	3821
DF	P2	FLD-SOS	pct50	0.939	11.6	10.5	0.794	3821
DF	P2	FLD-SOS	pct20	0.942	8.8	7.5	0.678	3821
DF	P2	FLD-SOS	pct10	0.945	9.9	8.6	0.602	3821
DF	P1	LCD-EOS	mean	0.618	39.3	37.9	0.577	3710
DF	P1	LCD-EOS	pct50	0.640	42.7	41.3	0.557	3748
DF	P1	LCD-EOS	pct80	0.658	35.5	34.1	0.579	3699
DF	P1	LCD-EOS	pct90	0.664	32.9	31.5	0.563	3663
DF	P2	LCD-EOS	mean	0.857	21.3	19.7	1.086	3731
DF	P2	LCD-EOS	pct50	0.866	24.7	23.4	1.069	3772
DF	P2	LCD-EOS	pct80	0.884	17.8	16.3	1.082	3703
DF	P2	LCD-EOS	pct90	0.874	15.1	13.5	0.968	3664
MF	P1	FLD-SOS	mean	0.407	35.8	30.1	0.368	1808
MF	P1	FLD-SOS	pct50	0.412	35.8	30.3	0.373	1808
MF	P1	FLD-SOS	pct20	0.353	33.5	25.3	0.300	1808
MF	P1	FLD-SOS	pct10	0.362	33.5	24.6	0.292	1808
MF	P2	FLD-SOS	mean	0.377	28.5	18.8	0.313	1659
MF	P2	FLD-SOS	pct50	0.362	28.9	19.3	0.299	1659

MF	P2	FLD-SOS	pct20	0.370	30.8	19.4	0.296	1659
MF	P2	FLD-SOS	pct10	0.388	33.4	22.2	0.294	1659
MF	P1	LCD-EOS	mean	0.245	43.9	37.0	0.202	1559
MF	P1	LCD-EOS	pct50	0.275	44.1	37.5	0.246	1559
MF	P1	LCD-EOS	pct80	0.223	47.2	41.0	0.153	1559
MF	P1	LCD-EOS	pct90	0.190	48.5	41.6	0.128	1559
MF	P2	LCD-EOS	mean	0.312	41.9	33.7	0.312	1647
MF	P2	LCD-EOS	pct50	0.331	38.9	31.8	0.358	1647
MF	P2	LCD-EOS	pct80	0.264	51.9	40.2	0.218	1647
MF	P2	LCD-EOS	pct90	0.233	56.2	43.1	0.187	1647
EF	P1	FLD-SOS	mean	0.407	39.5	35.0	0.603	1507
EF	P1	FLD-SOS	pct50	0.445	38.2	33.6	0.651	1507
EF	P1	FLD-SOS	pct20	0.324	35.9	30.7	0.478	1522
EF	P1	FLD-SOS	pct10	0.290	35.2	29.3	0.429	1529
EF	P2	FLD-SOS	mean	-0.269	49.6	42.7	-0.326	1670
EF	P2	FLD-SOS	pct50	-0.232	51.4	44.7	-0.274	1666
EF	P2	FLD-SOS	pct20	-0.295	57.9	50.9	-0.366	1683
EF	P2	FLD-SOS	pct10	-0.281	61.5	54.6	-0.351	1693
EF	P1	LCD-EOS	mean	0.536	38.9	29.1	0.654	2032
EF	P1	LCD-EOS	pct50	0.495	38.5	29.0	0.585	2033
EF	P1	LCD-EOS	pct80	0.469	48.2	37.9	0.550	2029
EF	P1	LCD-EOS	pct90	0.463	51.8	40.5	0.572	2031
EF	P2	LCD-EOS	mean	0.226	86.6	76.0	0.280	1562
EF	P2	LCD-EOS	pct50	0.247	79.6	68.6	0.307	1562
EF	P2	LCD-EOS	pct80	0.136	100.3	88.7	0.164	1562
EF	P2	LCD-EOS	pct90	0.102	105.6	94.1	0.127	1558

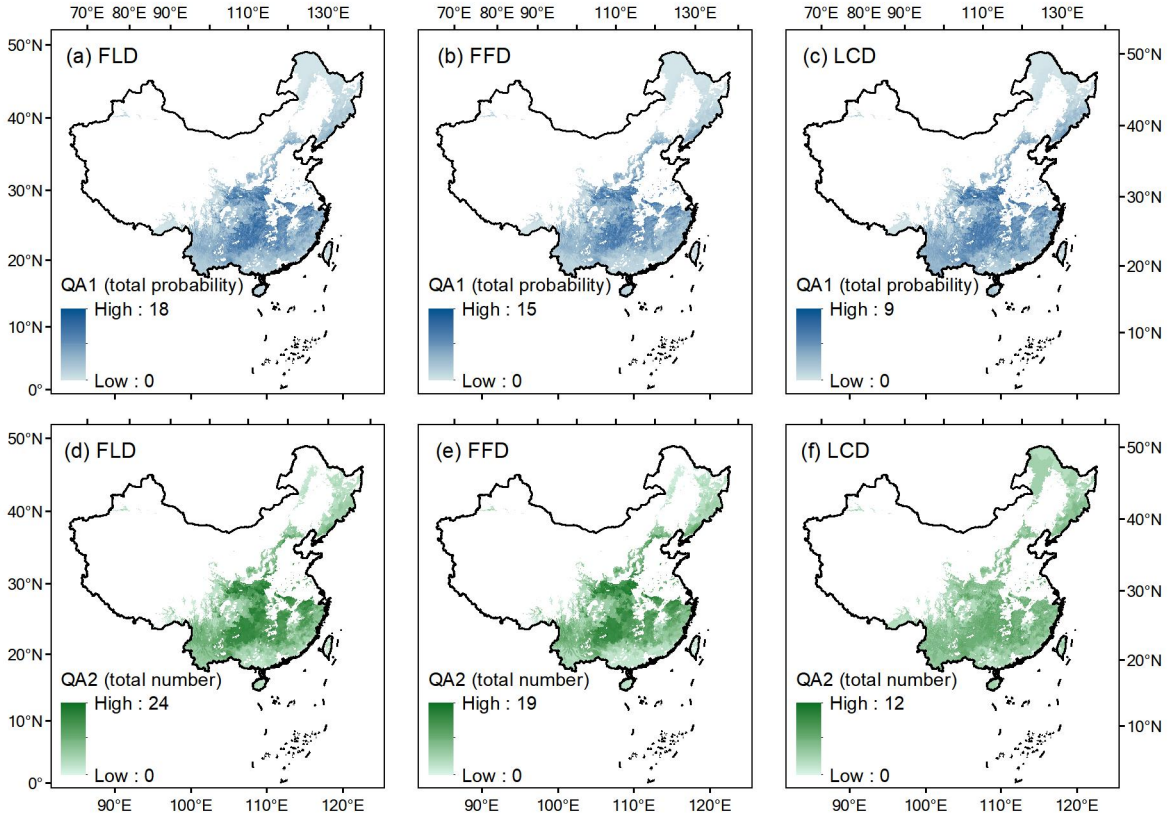

Figure S1: Quality assurance (QA) maps used to evaluate the reliability of the aggregation results of GP maps. (a-c) QA1 maps of FLD, FFD and LCD, showing the total distribution probability of all species. (d-f) QA2 maps of FLD, FFD and LCD, showing the total number of species with distribution probabilities greater than 0.1.

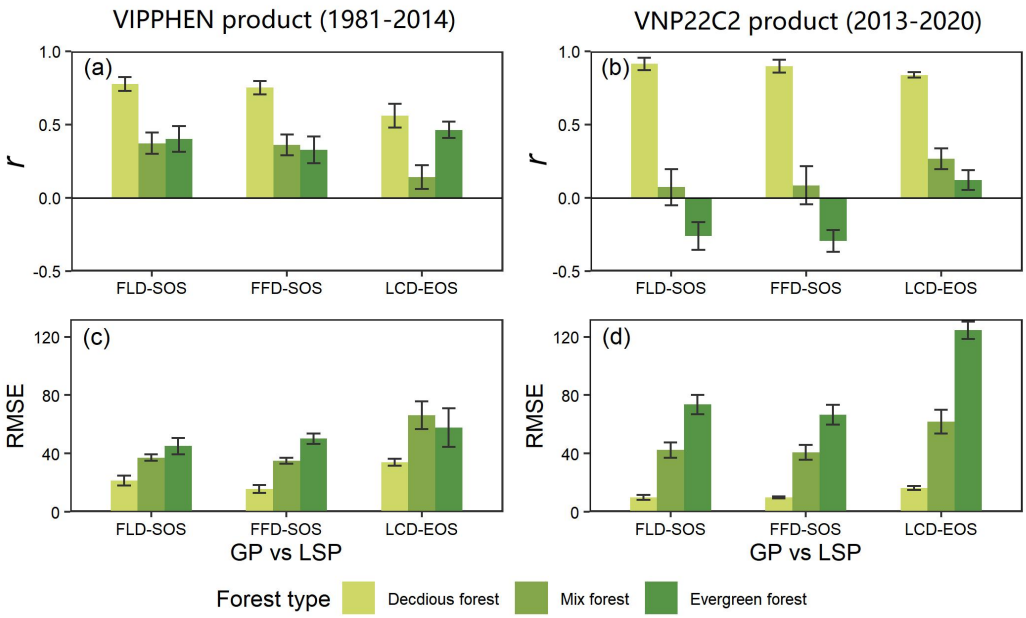

Figure S2: Comparison results of GP maps and two LSP products (VIPPHEN and VNP22C2) in different forest type areas, which was made between FLD (or FFD) and SOS in spring and between LCD and EOS in autumn within the time range 1981-2014 and 2013-2020. (a-b) R between LSP and GP under the best aggregating method in three forest types; (c-d) RMSE between LSP and GP under the best aggregating method in three forest types. Each forest type is represented by a different color. The error bar in the bar plot represents the multi-year standard deviation.

S1: Model formulations of three spring phenology models (Unichill, Unified, temporal-spatial coupling (TSC)), and two autumn phenology models (the multiple regression (MR) model, temperature-photoperiod (TP)).

(1) Unichill model: the model divides the process of bud burst into two phases: dormancy and quiescence, with nine species-specific parameters (*a, b, c, d, e, w, k, C** and t_c) fitted on phenological observations (Chuine, 2000). Parameters *a*, *b*, and *c* define the response function of chilling units ($R_c(x_t)$; eq. (1)). Parameters *d* and *e* define the response function of forcing units ($R_f(x_t)$; eq. (2)). Parameter t_0 is the time when $R_c(x_t)$ begins to accumulate, which determines the threshold of chilling accumulation (*C**; eq. (3)). Parameters *w, k,* t_c determine the threshold of the forcing accumulation (*F**; eq. (4)). When it reaches the threshold, the time t_b is FLD or FFD.

$$R_c(x_t) = \frac{1}{1+e^{a(x_t-c)^2+b(x_t-c)}} \tag{1}$$

$$R_f(x_t) = \frac{1}{1+e^{d(x_t-e)}} \tag{2}$$

$$\sum_{t_0}^{t_1} R_c(x_t) = C^* \tag{3}$$

$$\sum_{t_1}^{t_b} R_f(x_t) = F^*, \text{ where } F^* = we^{kC_{tot}}, \quad C_{tot} = \sum_{t_0}^{t_c} R_c(x_t) \tag{4}$$

(2) UniChill model: it is a simplified version of Unified model, which contains seven parameters: *a*, *b*, *c*, *d*, *e, C** and *F** (Chuine, 2000). On the basis of Unified model, this model fixes the start time t_1 for of the forcing unit as September 1 of the previous year, and fixes the forcing accumulation (*F**) required for the start of the spring phenology every year.

(3) TSC model: the model is built on SW model (Hunter and Lechowicz, 1992; eq. (5, 6)) , which uses the winter average temperature to determine the threshold of the forcing accumulation (Ge et al., 2014; eq. (7)). The model includes six parameters: T_{b1}, *F**, t_0, *a*, *b* and *f*. $R_f(x_t)$ is the forcing unit, x_t is the average daily temperature on day *t*, and T_{b1} is the critical temperature. *F** is the threshold value of temperature accumulation. The temperature accumulation threshold F_i of different sites is determined by the winter (December of the previous year to February) temperature $\overline{T}_i^{WI}$ of site *i* and parameters *a*, *b*, *f*. Parameter t_0 is the time when the forcing unit begins to accumulate, and the time *y* is FLD or FFD when it reaches *F**.

$$R_f(x_t) = \begin{cases} 0 & x \le T_{b1} \\ x_t - T_{b1} & x \ge T_{b1} \end{cases} \tag{5}$$

$$\sum_{t_o}^{y} R_f(x_t) = F^* \tag{6}$$

$$F_i = a + b \times e^{\frac{\overline{T}_i^{WI}}{f}} \tag{7}$$

(4) MR model: the influence of average temperature on autumn LCD is discrepant in different months. The rising temperature in May and June may lead to the advance of LCD, while the rising temperature in August and September may lead to the delay of LCD (Estrella and Menzel, 2006). A multiple regression model (eq. (8)) was established based on the correlation (R_5-R_9) between LCD (P_l) and average temperature from May to September (T_5-T_9), where *a, b, c, d* and *e* are model coefficients and ε is constant term.

$$P_l = aT_5 + bT_6 + cT_7 + dT_8 + eT_9 + \varepsilon, \text{ if } \left|R_{5,6,7,8,9}\right| < 0.3 \quad a,b,c,d,e = 0 \tag{8}$$

(5) TP model: assuming that the autumn LCD is affected by both temperature and photoperiod (Delpierre et al., 2009). When photoperiod is lower than the threshold P_{start}, cold state $CDD(d)$ starts to accumulate (eq. (9)). When the accumulated $iCDD(d)$ exceeds the threshold Y_{crit}, the day d is the exact date of leaf coloring (Y_{mod}, eq. (10)). Daily cold state $CDD(d)$ is co-determined by daily temperature $T(d)$ and daily photoperiod $P(d)$ (eq. (11,12)). The model includes five parameters: P_{start}, Y_{crit}, T_b, x and y.

$$iCDD(d) == \begin{cases} 0 & P(d) \geq P_{start} \\ CDD(d-1) + CDD(d) & P(d) < P_{start} \end{cases} \tag{9}$$

$$Y_{\text{mod}} = d, iCDD(d) \geq Y_{crit} \tag{10}$$

$$\text{if } P(d) < P_{start}, CDD(d) = \begin{cases} 0 & T(d) \geq T_b \\ [T_b - T(d)]^x \times f[P(d)]^y & T(d) < T_b \end{cases} \tag{11}$$

$$f[P(d)] = \frac{P(d)}{P_{start}} \quad \text{or} \quad f[P(d)] = 1\text{-}\frac{P(d)}{P_{start}} \tag{12}$$

Where x and y can take values 0, 1 or 2 respectively. Among them, x=0 or y=0 indicates that LCD is independent of temperature or photoperiod; x=1 or y=1 indicates that LCD is linearly related to temperature or photoperiod; x=2 or y=2 indicates a nonlinear correlation with temperature or photoperiod.

References

Chuine, I.: A unified model for budburst of trees, J. Theor. Biol., 207, 337–347, https://doi.org/10.1006/jtbi.2000.2178, 2000.

Delpierre, N., Dufrêne, E., Soudani, K., Ulrich, E., Cecchini, S., Boé, J., and François, C.: Modelling interannual and spatial variability of leaf senescence for three deciduous tree species in France, Agric. For. Meteorol., 149, 938–948, https://doi.org/10.1016/j.agrformet.2008.11.014, 2009.

Estrella, N. and Menzel, A.: Responses of leaf colouring in four deciduous tree species to climate and weather in Germany, Clim. Res., 32, 253–267, https://doi.org/10.3354/cr032253, 2006.

Hunter, A. F. and Lechowicz, M. J.: Predicting the timing of budburst in temperate trees, J. Appl. Ecol., 597–604, https://doi.org/10.2307/2404467, 1992.

Ge, Q., Wang, H., and Dai, J.: Simulating changes in the leaf unfolding time of 20 plant species in China over the twenty-first century, Int. J. Biometeorol., 58, 473–484, https://doi.org/10.1007/s00484-013-0671-x, 2014.